Applied Thermal Engineering 199 (2021) 117518

Contents lists available at ScienceDirect

Applied Thermal Engineering

journal homepage: www.elsevier.com/locate/ate

Research paper

Control-oriented modelling and operational optimization of a borehole thermal energy storage

Massimo Fiorentini [a,*], Luca Baldini [b]

[a] Urban Energy Systems Laboratory, Empa - Swiss Federal Laboratories for Materials Science and Technology, 8600 Dübendorf, Switzerland
[b] Zurich University of Applied Sciences, 8401 Winterthur, Switzerland

ARTICLE INFO

Keywords:
Seasonal thermal energy storage
Borehole thermal energy storage
Operational optimization
Seasonal load shift
Energy flexibility
CO2 emissions reduction

ABSTRACT

Seasonal thermal energy storage is an effective measure to enable a low carbon future through the integration of renewables into the energy system. Borehole thermal energy storage (BTES) provides a solution for long-term thermal energy storage and its operational optimization is crucial for fully exploiting its potential. This paper presents a novel linearized control-oriented model of a BTES, describing the storage temperature dynamics under varying operating conditions, such as inlet temperature, mass-flow rate and borehole connection layouts (e.g. in-series, in-parallel or mixed). It supports an optimization framework, which was employed to determine the best operating conditions for a heat pump-driven BTES, subject to different CO_2 intensity profiles of the electricity. It was demonstrated that this boundary condition, due to its seasonal variation, is critical for the optimal operation of the system, as increasing heat pump efficiency in winter while accepting a lower one in summer can be beneficial. Results for an exemplary district case, subject to two different CO_2 intensity profiles, show that a lower relative intensity in summer compared to the one in winter leads to a higher optimal operating temperature of the storage. The district system studied is heating-dominated, effectively enabling the BTES to cover only 20% of the total heat demand, leading to limited total yearly CO2 emissions savings of 2.2% to 4.3%. When calculating the benefits associated with the heating and cooling demand handled by the BTES, a higher CO_2 emission reduction in the range of 12.8%–19.9% was found. This highlights the BTES potential when subject to more balanced loads.

1. Introduction

Global energy demand for heat represents almost half of final energy demand, as reported by the IEA [1]. Demand for heat, according to this report, was higher than the final energy need for electricity and transport combined. Energy storage technologies provide an effective mean for achieving a low-carbon future, as they allow a decoupling of energy supply and demand, and mitigate of the mismatch between renewable energy sources (RES) generation and demand.

A temporal mismatch between solar generation and demand occurs on both a daily and seasonal basis. Daily mismatches can be mitigated with short-term energy storage devices, however seasonal mismatches, which are particularly evident in heating-dominated climates, require longer term storage solutions. Several seasonal storage options are available, as presented in [2], which provided a review of the different seasonal thermal energy storage technologies that are feasible for district heating applications, and highlighted the advantages and drawbacks of each. A review with more focus on recent developments in energy storage solutions in the ground using ground heat exchanger (GHX)s was performed in [3], as this type of storage technique has proven to be cost-effective, especially at large scales [4].

To minimize the heat losses to the surrounding undisturbed underground, ground source heat pump (GSHP) systems generally operate BTES at low charging and discharging temperatures. When implemented in newer generation district thermal networks, often referred to as 5th generation district heating and cooling systems, they enable buildings to become prosumers as in an electrical smart grid [5].

Increasing the temperature of the BTES leads to an increase in thermal losses, but at the same time increases the efficiency of the discharging system in winter [6]. This can be important in deciding how to operate a BTES, as a significant seasonal variation in CO_2 emissions per kWh generated can be present between summer and winter [7]. For this reason, high temperature BTES are studied in [8], with the aim of seasonal load shifting for improving winter heat pump performance and thus reduced yearly CO_2 emissions. If the temperature of the storage is high enough and coupled with low-temperature heating systems such as in [9], it is also possible to directly supply heat

* Corresponding author.
E-mail address: massimo.fiorentini@empa.ch (M. Fiorentini).

https://doi.org/10.1016/j.applthermaleng.2021.117518
Received 25 May 2021; Received in revised form 15 July 2021; Accepted 29 August 2021
Available online 7 September 2021

Nomenclature

T_{in}	Supply temperature to the BTES (°C)
T_a	Air temperature above ground (°C)
T_{ij}	Temperature of ground capacitances (°C)
T_g	Initial and undisturbed ground temperature (°C)
$\dot{m}$	Heat transfer fluid mass flow rate (kg/s)
c_p	Heat transfer fluid specific heat capacity (kJ/kg K)
k_{gr}	Ground thermal conductivity (kW/m K)
C_{ij}	Ground capacitance element (KWh/K)
$R_{b_{id}}$	Identifiable borehole thermal resistance per unit of pipe length (K/m W)
R_{hij}	Ground horizontal resistance element (K/kW)
R_{vij}	Ground vertical resistance element (K/kW)
D	Storage depth (m)
d_i	Depth of ground layers (m)
r_j	Radii of cylinder sections (m)
δ	Boolean variable that activates BTES operating modes and pump speeds (−)
l_p	Length of u-pipe (m)
ρ	Heat transfer fluid density (kg/m^3)
P_{th}	Heat transfer via the boreholes (kW)
$P_{el,c}$	Electrical power consumption for circulation in the BTES (kW)
P_{el}	Electrical power consumption of the heat pump (kW)
P_{load}	Net thermal load available to the BTES (kW)
COP_{ch}	Coefficient of performance in charging (kW)
COP_{dis}	Coefficient of performance in discharging (kW)

Acronyms

BTES	borehole thermal energy storage
RES	renewable energy sources
STTS	short-term thermal storage
GHX	ground heat exchanger
GSHP	ground source heat pump
NLP	non-linear programming
AMTD	arithmetic mean temperature difference
LMTD	logarithmic mean temperature difference
MIP	mixed integer programming
HTF	heat transfer fluid

from the storage. Nevertheless, high-temperature systems are subject to design and operation problems that are not present in low-temperature systems [10], but it is nowadays possible to overcome them. BTES systems are often combined with short-term thermal storage (STTS) to provide a buffer for daily demand, and mitigate peaks in generation that could not otherwise be transferred to the BTES due to its limited heat transfer rate [11–13].

Several mathematical models have been formulated to determine the performance of a BTES system, accounting for both the large-scale heat transfer in the ground volume and the local processes in and around the borehole. A comprehensive review of the currently available simulation models available and implemented in commercially available software is presented in [14]. The Superposition Borehole Model (SBM) [15] is a detailed and experimentally validated [16,17] finite-difference model that allows the evaluation of a BTES in an arbitrary configuration. This model has also been used to calculate dimensionless thermal response functions for defined configuration fields, used for fast performance estimates in approaches such as in the EED software [18]. Recent studies focused on the development of a semi-analytical method for the calculation of g-functions of bore fields with mixed arrangements of in-series and in-parallel BTES plumbing configurations [19], as well as a full-time-scale semi-analytical bore field simulation model, enabling the simulation of BTES with arbitrarily positioned boreholes, capable of accounting for both short-term and long-term thermal interactions [20]. A faster computational model, designed to be integrated in the Modelica modelling language was also proposed in [21].

Optimizing the charging and discharging conditions of the BTES is critical in ensuring that the maximum amount of heat available to be stored is transferred to the ground and effectively extracted later in the year, using the least amount of electrical energy possible for water circulation in the GHXs. Optimizing their capacity is also important for ensuring the economic feasibility of these systems, as they require a high investment cost [22]. The plumbing arrangement is also important, as an in-series configuration of the individual GHXs, compared to an in-parallel one, would generate a temperature gradient from the core to the periphery of the storage. This temperature gradient will reduce the thermal losses and require a lower mass flow rate of heat transfer fluid (HTF), but at the same time require a higher charging temperature (and therefore lower heat pump COP) due to the higher core temperature, and can therefore limit the exploitation of the full ground capacitance. In general, for optimization of thermal storages simplified and reliable modelling methods are required, such as described in [23], developed to optimize a stratified water storage with solar collectors, or as described in [24], where four approaches to model stratification in thermal energy storage were compared with the aim to be optimized with mixed-integer linear programs.

To predict the performance of a seasonal thermal storage system for optimization purposes, its thermal behaviour is generally modelled in detail. Advanced heat transfer models that focus on the behaviour of the subsurface within and surrounding the BTES system have been developed, for example using finite element-based software models then verified against a scaled experimental setup [25], or against data from operating systems such as the one developed for the Drake Landing solar community [26]. In [27] for example, the response of a BTES with a controllable inlet position was simulated with the support of a CFD analysis, and in [28] the seasonal storage was simulated with detailed modelling undertaken in TRNSYS [29] and optimized with an evolutionary approach (Genetic Algorithm NSGA-II) performed with the Multi-Objective Building Optimization (MOBO) tool. Similarly, in [30], the design of a seasonal thermal tank storage, modelled in TRNSYS, was optimized using a hybrid meta-heuristic algorithm part of the tool GenOpt. A study conducted at a residential scale [31] optimized a building-integrated solar thermal system with seasonal storage using a parametric analysis of the system, also using TRNSYS. The downside of the approach taken by these studies is that these modelling methods do not allow the application of numerical optimization methods, and finding the optimal solution in an iterative manner might always not be possible. For example, in [32], operational data of a BTES was used to calibrate a heat transport model in FEFLOW, but the application of conventional optimization techniques was not feasible due to long computational times, and a manual iteration technique was applied instead. In district-scale studies aiming at optimizing energy resources and their power dispatch, to allow numerical optimization of the design problem, BTES systems are often modelled simply as a single capacitance with a nominal efficiency, as in [33] and [34]. With this simplified modelling, the effect of the HTF inlet temperature and flow rate on the heat exchange with the ground cannot be taken into consideration. This can lead to erroneous estimations of the possible heat transfer rate and

BTES temperature, and with it the temperature-dependent performance of supporting equipment such as heat pumps. An alternative one-dimensional analytical model of a single GHX was presented in [35], developed using the Green's function method, with the intent of using it for design purposes. A simplified linear model for a single borehole model was proposed [36] for real-time optimization. An optimization method based on an extension of dual dynamic programming with application to nonlinear energy storage was proposed in [37], solving the operational problem for a single borehole system with a heat pump. In [38], using temporally and spatially superimposed line source equations, an optimization method to find an optimal arrangement of in-parallel GHXs for a given seasonal energy demand was presented. A similar, more detailed approach, was undertaken in [39], where a simulation study assessed the impact of the COP formulation of a GSHP and a borehole model for model predictive control of a hybrid geothermal system, resulting in a non-linear programming (NLP) problem. The operational optimization of a BTES, together with other energy system components, was undertaken in [40], capturing the short- and long-term dynamics of energy conversion, storage and consumption. It is based on g-functions to estimate the dynamic response of the BTES. The efficiency of the heat pumps and the energy output of the heat exchangers required linearization to reduce the complexity to a MILP problem. In [41] the design optimization was approached using a Neural Network metamodelling, trained on a TRNSYS model, and compared and combined with a Genetic Algorithm (NSGA-II).

1.1. Research gap and contribution

This paper provides an effective modelling and operation optimization methodology for a BTES field, to reduce the yearly CO2 emissions of a district heating and cooling system by using the seasonal storage to shift the electricity loads of a heat pump from periods with a high CO2 intensity (typically winter) to periods with a lower intensity (summer). The novel contribution of this paper is to provide an optimization methodology to determine the best operating conditions for a heat pump-driven BTES, subject to different yearly CO_2 intensity profiles of electricity supply. It is demonstrated that this boundary condition is critical in determining the optimal operation of the system (e.g. operating the BTES at low or high temperature). To enable this numerical optimization, a control-oriented model is required, with the capability to describe the effects on the electric load of the heat pump and circulation system of parameters including the BTES plumbing configuration (in-series or in-parallel or mixed — allowing mode switching), supply temperature and flow rate to the BTES,. To the best of the authors' knowledge there is a gap in current research, as such a control-oriented model is currently not available in the literature. The existing BTES modelling methods that describe the field response in relation to the variation of these parameters – in particular switching plumbing configuration during operation – are not suitable for numerical optimization.

For this purpose, this study proposes a linearized modelling method for the storage dynamics, based on a resistance–capacitance (R–C) equivalence and linearized heat transfer calculation within the boreholes, which is then calibrated and validated against a high-fidelity TRNSYS model. This model, differently from other modelling techniques available in the literature, allows for the estimation of the thermal response of the ground with dynamically changing inlet temperatures, flow rates and plumbing configurations, in conjunction with the expected consumption for the circulation of the HTF. Coupling this model with a linearized expression for the inverse of the heat pump's COP, a bilinear optimization problem is obtained, which enables the possibility to find an optimal open-loop solution for a system under defined boundary conditions.

This methodology is demonstrated on a case study district heating and cooling system in place and a BTES to be built. For this case, the aim was to demonstrate how different CO_2 emissions intensity profiles affect the optimal operation of the BTES storage.

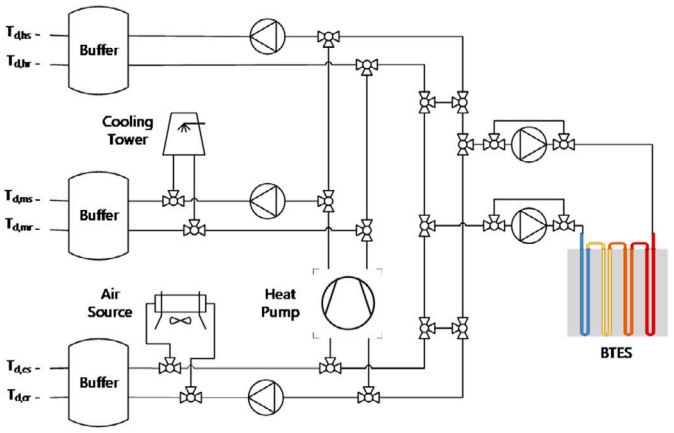

Fig. 1. Empa campus heating and cooling network.

2. Case study

2.1. Energy system

The case study used in this work is the Empa research campus in Dubendorf, Switzerland, which includes 35 buildings of different use (e.g. office, laboratory, etc.) and require both heating and cooling throughout the year. The thermal energy, currently generated with a natural gas boiler and a chiller, is distributed to the buildings using three networks at different temperatures, as presented in the study by Weber and Baldini [8]. The high-temperature network supplies heat at 65 °C, the mid-temperature network, which is used for both low-temperature heating and heat rejection, operates at 35 °C and the cold network, which is also used as a source for the heating operations, supplies cooling at 6 °C.

In the course of the renewal of the campus energy system, a heat pump will provide the base heating load and a BTES will be installed to use the waste heat from cooling to charge the storage. In this study, the system was slightly simplified, removing the auxiliary gas heater and assuming a heat pump with infinite capacity, able to supply all the required demand for heating and cooling throughout the year, as well as to generate the heat to be transferred to the BTES. The system schematic is presented in Fig. 1.

It is assumed that the heat rejected from the cooling operations is exhausted via a cooling tower, if it cannot be stored in the BTES. It is also assumed that the supply temperature to the BTES can be controlled using recirculating water via the 3-way valves in Fig. 1, constrained to 65 °C in charging and 12 °C in discharging.

The different networks with distinct temperature levels available facilitate the integration of a BTES with temperatures well above the natural soil temperatures. The yearly heating and cooling demand of the Empa campus is presented in Fig. 2. The heating load contains both high and medium temperature heating loads. Because the majority of the building on this campus is relatively old, a large portion of the heating load is at high temperature. For simplicity, in this study, it is thus assumed that all the demand is for heating at the high-temperature level. In future, a larger fraction of low-temperature heating demand would increase the performance benefit using a high-temperature BTES.

The demand of the campus was averaged over each week, to serve as an input (P_{load}) to the model developed in this study. P_{load} is assumed to have the opposite sign to the demand in Fig. 2, being positive when the BTES is charged and negative when it is discharged.

2.2. BTES design

The proposed BTES field, based on an initial design constrained by the space available within the Empa campus, includes 144 double-U

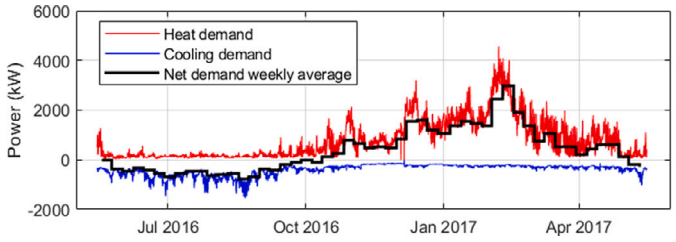

Fig. 2. Empa campus heating and cooling demand and CO_2 emissions intensity of the Swiss grid.

Table 1
BTES construction parameters.

Parameter	Value
Borehole diameter (m)	0.14
U-pipe diameter (m)	0.04
U-pipe thickness (m)	0.0032
U-pipe thermal conductivity (W/m K)	0.35
U-pipe shank spacing (m)	0.06
U-pipe starting depth (m)	1
U-pipe length (m)	50
Filling thermal cond. (W/m K)	0.6
Contact resistance pipe/filling (m K/W)	0.02
Heat conductivity ground layer (W/m K)	2.4
Volumetric heat capacity ground layer (kJ/K m^3)	2200
Heat transfer coefficient air to ground (W/m^2 K)	0.08
Initial ground temperature (°C)	12

GHXs, 50 meters deep, and with a layer of insulation above the borehole field. The construction details of the BTES and the heat exchangers are summarized in Table 1. For simplicity, for all the simulations, the ground is assumed to be of uniform rock material at a constant initial temperature and without an initial depth-related temperature gradient. A temperature response test conducted on-site did not highlight the presence of groundwater flow.

The GHX field is assumed to be either connected with 18 in-parallel circuits with 8 GHXs in-series as per the proposed layout presented in [8] and shown in Fig. 3, or with all the GHXs connected in parallel. The parallel topology represents the classical design of low-temperature BTES and can be taken as the reference case for this study. The GHXs are located at a distance of 4 m from each other, in a triangular pattern. Consequently, they are homogeneously distributed, and each borehole has equal volume of ground for thermal interaction. The sections delimited by the circles in Fig. 3 divide the cylinders into eight equal volumes and contain on average the same number of GHXs, belonging to each one of the loops in the in-series configuration, from first to the eighth.

3. BTES modelling methodology

To enable a simplification of the BTES modelling for optimization purposes, it is assumed that the BTES volume is cylindrical, that ground properties are uniform and there is no groundwater flow, that the boreholes are evenly distributed, and that the volume of the storage can be separated in several slices equal to the number of parallel channels of the plumbing configuration. Under these assumptions, each slice of the cylinder (Fig. 4) does not exchange heat with the neighbouring ones as they are at the same temperature, and therefore results from modelling only one portion can be extrapolated to the whole system. The portion under consideration can be further divided into a number of sections, equal to the number of in-series connections of the plumbing configuration, as presented in Fig. 4.

Each of the capacitances is taken to be in the middle of the section, with each resistance calculated using the annular conduction

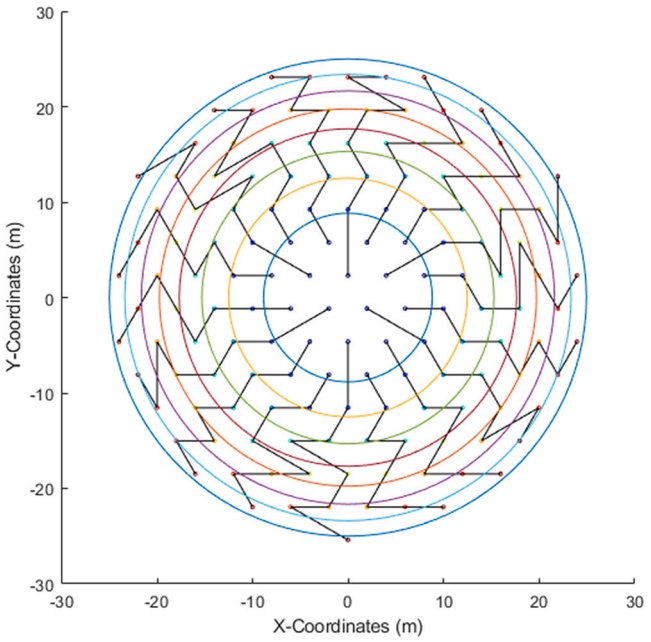

Fig. 3. Borehole coordinates and volumes of the case study BTES storage, based on the configuration presented in [8].

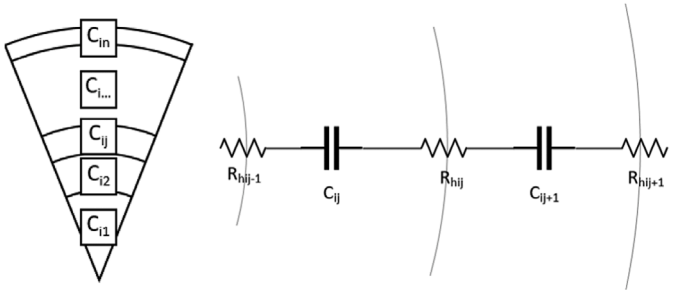

Fig. 4. Resistances in section of BTES cylinder.

relationship in Eq. (1).

$$R_{hij} = \frac{\ln\left(\frac{r_{j+1}}{r_j}\right)}{2\pi k_{gr} d_i} \tag{1}$$

where d_i is the depth of the ground layer, r_j are the radii of the sections of the cylinder, k_{gr} is the ground thermal conductivity.

This concept can be extended around and below the BTES volume, creating a resistance–capacitance (R–C) network, as presented in Fig. 5, with the vertical resistances calculated assuming linear heat conduction. Each capacitance and resistance can be denoted with the index i for each vertical element, and j for each horizontal element. Each capacitance C_{ij} is connected to the previous and next horizontally distributed capacitances via the resistances R_{hij} and to the capacitances above and below via the resistances R_{vij}. At the boundary conditions, the capacitances are connected either to the ambient air T_a, as in the case of the first layer, or to the undisturbed ground temperature T_g. Details on the number of sections used to model the case study BTES and their dimensions are described in the implementation section (Section 5). As the HTF circulates through the pipes in the borehole, it exchanges heat with the ground, and the amount of heat exchanged depends on the configuration of the heat exchangers and the conditions of the fluid. The heat transfer through the GHXs is represented in Fig. 5 by the generators $P_{11}, \ldots, P_{1n}$. It is assumed that only the first n capacitances of the first row are subject to a power input and therefore

model the BTES volume, while the rest of the capacitances model the near-field dynamical effects.

Assuming a total number of states equal to N_{st}, represented by the volume capacitances and temperatures, the evolution of the temperature distribution can be expressed as a linear state-space model of the form:

$$\begin{cases} \dot{x} = Ax + Bu \\ y = Cx + Du \end{cases} \tag{2}$$

where the state vector is $x = \left[T_{11}, \ldots, T_{1N}, T_{21}, \ldots, T_{2N}, T_{m1}, \ldots, T_{mN}\right]^T$, and the first N states of this vector represent the first layer of the simulated ground volume. The state matrix A, representing the ground dynamics without the effect of the GHXs, is (N_{st} x N_{st}) matrix of the form:

$$A = \begin{bmatrix} a_{1,1} & a_{1,2} & 0 & 0 & 0 & \cdots & 0 & a_{1,N+1} & 0 & 0 & 0 & \cdots & 0 \\ a_{2,1} & a_{2,2} & a_{2,3} & 0 & 0 & \cdots & 0 & 0 & a_{2,N+2} & 0 & 0 & \cdots & 0 \\ 0 & \ddots & \ddots & \ddots & 0 & \cdots & 0 & 0 & 0 & \ddots & 0 & \cdots & 0 \\ \vdots & & \ddots & \ddots & \ddots & & & & & & \ddots & & \vdots \end{bmatrix} \tag{3}$$

where for example, each row of matrix A contains in general elements a as in Eq. (4):

$$\begin{cases} a_{p,p-1} = \frac{1}{C_{1j-1} R_{h1j-1}} \\ a_{p,p} = \frac{1}{C_{1j}} \left(\frac{1}{R_{h1j-1}} + \frac{1}{R_{h1j}} + \frac{1}{R_{v1j-1}} + \frac{1}{R_{v1j}} \right) \\ a_{p,p+1} = \frac{1}{C_{1j} R_{h1j}} \\ a_{p,p+N} = \frac{1}{C_{1j} R_{v1j}} \\ a_{p,p-N} = \frac{1}{C_{1j} R_{v1j-1}} \end{cases} \tag{4}$$

where $p = (i-1)N + j$ is an index defined for iterating through the N_{st} elements of the state vector.

These elements slightly vary when they are close to a boundary condition of the modelled volume. For example, the first N rows, which represent elements connected to the ambient air via the top insulation resistance, do not have an element $a_{i,j-N}$, and the element $a_{j,j}$ contains the top layer resistance $R_{e,j}$, instead of the connection resistance to another ground volume R_{v1j-1} as in Eq. (5):

$$a_{p,p} = \frac{1}{C_{1j}} \left(\frac{1}{R_{h1j-1}} + \frac{1}{R_{h1j}} + \frac{1}{R_{e,j}} + \frac{1}{R_{v1j}} \right) \tag{5}$$

Similarly, the last N rows are also slightly different, as they represent elements connected to the undisturbed ground temperature. The vertical resistance in the element $a_{p,p+N}$ would not be present in the state matrix, but in the input matrix as described below.

To include the heat transfer through the GHXs in the state-space formulation in Eq. (2), it requires it to be also expressed linearly. The numerical model proposed by Eskilson [15] described the u-tube GHXs heat transfer connecting the upward and downward-flowing pipes through resistances in a delta configuration, expressing the outlet temperature of the heat exchanger as a linear function of the inlet and the borehole wall temperature, under the assumption that the coefficients of this relationship are a function of the flow rate.

In this paper, we propose a linear approach for the calculation of the outlet temperature and heat exchange for a defined pump speed, which can be added to the linear dynamical model of the ground. This is done without relying on knowledge of the exact construction of the heat exchanger, making this approach also suitable for application in existing systems. The proposed heat exchange is reduced to one of a single pipe exposed to a constant temperature equal to the one of the capacitance in which the GHX is located. This approach would over-estimate the heat exchange to the ground, as the thermal connection between the downwards flowing section of the pipe and the upwards flowing one (as described in detail in the modelling proposed by Bauer [42]) is neglected. Therefore, a lumped "identifiable" resistance of the borehole $R_{b,id}$ is included in the estimation of the total heat transfer coefficient of this equivalent pipe. This lumped resistance includes the borehole filling, pipe material and contact resistances, and adds to the one linked to the forced convective heat exchange R_c, which is calculated using a constant Nusselt (Nu) number for the laminar regime (3.66) and the Gnielinski correlation for the transient and turbulent regimes ($Re > 2500$). This identifiable resistance approach is not only useful to correct the proposed simplified modelling, but it can calibrated to real systems and absorb uncertainties related with physical construction and operation. The value of $R_{b,id}$ is identified by minimizing the root-mean-square error (RMSE) between the predicted power delivery of the BTES and the measured one, or the more accurate one calculated via more time consuming simulation. The value of $U_{b,tot}$ is then calculated as $1/(R_{b,id} + R_c)$ and used to derive the temperature at the outlet of each u-pipes as in Eq. (6), applying the logarithmic mean temperature difference:

$$T_{out} = T_{ij} - (T_{ij} - T_{in}) e^{\left(-\frac{l_p U_{b,tot}}{c_p \dot{m}}\right)} \tag{6}$$

This can be linearized for a defined system mass flow rate, assuming that the temperature difference between inlet and outlet section of the piping is small, and using the arithmetic mean temperature difference (AMTD) instead of the logarithmic mean temperature difference (LMTD) as in the expression in Eq. (7).

$$T_{out} = T_{in} K_1 + T_{ij} K_2 \tag{7}$$

where the coefficients K_1 and K_2 are presented in Eq. (8).

$$\begin{cases} K_1 = \frac{\dot{m} c_p - l_p U_{b,tot}/2}{\dot{m} c_p + l_p U_{b,tot}/2} \\ K_2 = \frac{l_p U_{b,tot}}{\dot{m} c_p + l_p U_{b,tot}/2} \end{cases} \tag{8}$$

The heat transfer P_{ij}, in both in-series and in-parallel BTES configurations, can be expressed linearly as a function of the states T_{ij} and an input variable T_{in}, which is the supply fluid temperature to the BTES.

Assuming the GHXs are connected in series in charging mode, and the fluid is flowing from the centre of the storage (at temperature T_{11}) towards its periphery, the heat transferred from the fluid to the BTES capacitances is equal to the expressions in Eq. (9):

$$\begin{cases} P_{11} = \dot{m} c_p (T_{in,1} - T_{out,1}) = \dot{m} c_p [(1 - K_1) T_{in} - K_2] T_{11} \\ P_{12} = \dot{m} c_p [(1 - K_1) K_1 T_{in} + K_2 (1 - K_1) T_{11} - K_2 T_{12}] \\ \vdots \\ P_{1n} = \dot{m} c_p [(1 - K_1) K_1^{n-1} T_{in} + K_2 (1 - K_1) K_1^{n-2} T_{11} + \\ \qquad + K_2 (1 - K_1) K_1^{n-3} T_{12} + \cdots - K_2 T_{1n}] \end{cases} \tag{9}$$

If the storage is in discharging mode, a similar set of equation as in Eq. (9) can be derived, starting from P_{1n} and calculating the heat transfer in each borehole towards the centre. If the connections are in parallel, each heat input P_{1j} is calculated as done for P_{11} in Eq. (9), using the different boundary temperature of each borehole T_{1j}.

This enables the calculation of several switchable linear systems, depending on the mode of operation and pump speed, which can be used for system optimization. The parts of each heat input P_{1j} in Eq. (9) that multiply state variables (e.g. T_{11} to T_{1n}) are added to the state matrix A, whether the coefficients that multiply T_{in} are to the input matrix B.

The continuous input vector for each linear system is therefore equal to $u_c = [T_{in}, T_a, T_g]^T$, and B is of size N_{st} x 3. The elements b of the first n rows of this matrix are equal to (Eq. (10)):

$$b(p,2) = \frac{1}{C_{1j-1} R_{e,j}} \tag{10}$$

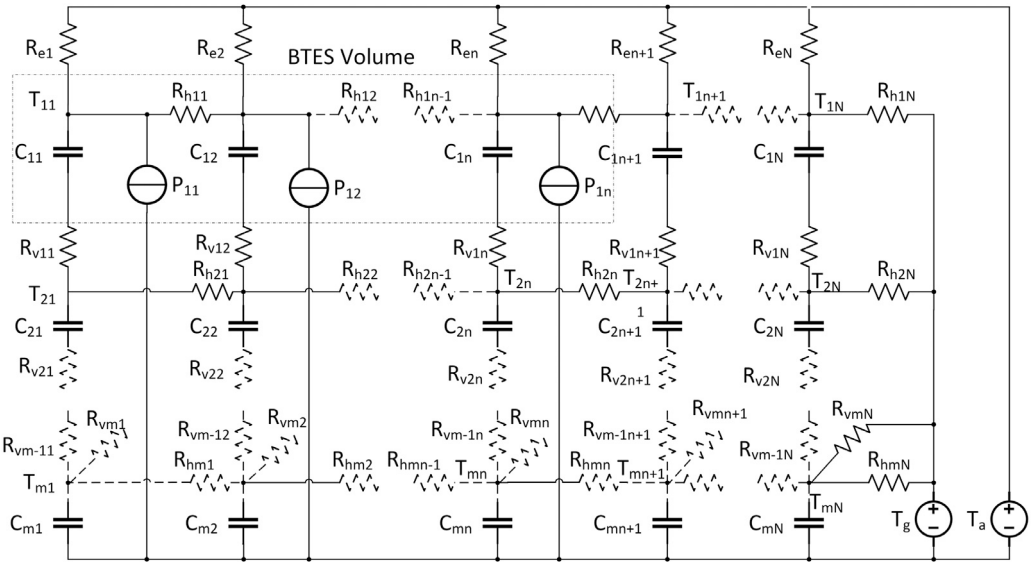

Fig. 5. BTES R–C model.

and when the states are connected to the undisturbed ground temperature on the side of the storage (e.g. when $j = N$ and when $i = m$) the elements are equal to (Eq. (11)).

$$b(p,3) = \frac{1}{C_{ij} R_{vij}} \tag{11}$$

As for the state matrix, the elements of each heat input P_{1j} in Eq. (9) that multiply the input variable T_{in} is added to the matrix B in the element $b(p,1)$.

Several linear systems can be defined to describe the dynamical behaviour of the BTES in a determined configuration (e.g. in-parallel, in series, pump speed), a discrete input array u_d that can switch between them can be defined. This vector u_d is equal to

$u_d = [\delta_{c,s1}, \delta_{d,s1}, \delta_{c,s2}, \delta_{d,s2}, \dots, \delta_{p1}, \delta_{p2}, \dots, \delta_{ff}]^T$, where the subscript c, s denotes an in-series charging configuration, d, s a in-series discharging configuration, p a parallel one and ff the free-floating (no mass flow through the BTES case).

The state-space systems that describe the BTES behaviour in each operating mode and pump speed can be therefore defined as in Eq. (12), where the heat transfer in each one of the BTES sections can be calculated as an output y by rearranging the elements of Eq. (9) in the matrices C and D:

$$\begin{cases} \dot{x} = A_{c,s1}x + B_{c,s1}u_c; & y = C_{c,s1}x + D_{c,s1}u_c & \text{if } \delta_{c,s1} \\ \dot{x} = A_{d,s1}x + B_{d,s1}u_c; & y = C_{d,s1}x + D_{d,s1}u_c & \text{if } \delta_{d,s1} \\ \quad\vdots & & \\ \dot{x} = A_{p1}x + B_{p1}u_c; & y = C_{p1}x + D_{p1}u_c & \text{if } \delta_{p1} \\ \quad\vdots & & \\ \dot{x} = A_{ff}x + B_{ff}u_c & y = C_{ff}x + D_{ff}u_c & \text{if } \delta_{ff} \end{cases} \tag{12}$$

As the hydraulic losses in each operating mode and pump speed are known, an energy cost can be assigned to each one of them to be included in an optimization cost function. At the same time, the number of operating mode scenarios to be evaluated in the optimization must remain limited to reduce computational complexity.

3.1. Hydraulic losses

The calculation of the hydraulic losses in the U-pipes is essential to determine the required electrical energy that has to be spent to achieve a predicted heat exchange to/from the BTES at each control time step. The total pressure drop in each section of the network dp_s, dependent on the system flow rate $\dot{V}$, can be calculated as the sum of pressure drop of minor and major losses:

$$dp_s(\dot{V}) = dp_{min}(\dot{V}) + dp_{maj}(\dot{V}) \tag{13}$$

as each section is effectively a GHX, the minor losses consist in this case of 90° bends to connect the GHXs piping and a 180° bend for the bottom of each u-pipe, while the major losses are calculated using the Darcy–Weisbach equation assuming a piping material roughness considered to be equal to $\epsilon = 1.52$ μm. The total pressure drop was then calculated for each BTES plumbing configuration, considering the different in-series and in-parallel arrangements.

Considering the mechanical power necessary to move the HTF in each the piping, and a nominal efficiency of the pump and electric motor η (assumed equal to 0.6 in this study), the electrical consumption is calculated as in Eq. (14).

$$P_{el,c}(\dot{V}) = \dot{V} dp_{tot}(\dot{V})/\eta \tag{14}$$

4. BTES control optimization

The modelling methodology presented in Section 3 can be effectively used for BTES system operational optimization. In this section a baseline controller that optimizes the flow rate through the BTES with constant inlet charging and discharging temperatures is firstly presented, to offer a reliable benchmark and an estimate of the best nominal flow range for the BTES to operate in. Secondly, a predictive control optimization is proposed, that can take into account future disturbances and the performance relationships of the energy conversion systems.

4.1. Baseline control: flow rate optimization

The thermal model of the BTES storage can be used to calculate, at each simulation/control time-step, the thermal power that can be supplied or extracted from the BTES volume as the sum heat transfer in each of the individual GHXs (P_{1j}), depending on the flow rate and system states as in Eq. (15).

$$P_{th}(\dot{V}, T) = \sum_{j=1}^{N} P_{1j}(\dot{V}, T_{1j}) \tag{15}$$

An objective function can be written so that the heat transfer to and from the BTES is maximized in comparison to the electrical power

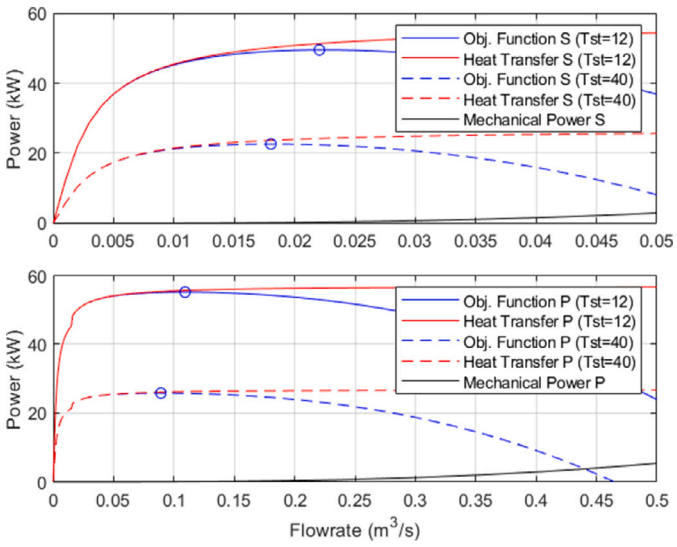

Fig. 6. Objective function evaluation (Matlab model) for $\alpha = 6$, with supply temperature equal to 65 °C and storage volume at a uniform temperature (T_{st}) of 12 °C or 40 °C for parallel (top) and in-series (bottom) arrangement of the GHXs. The blue circle is marking the maximum of the objective function and the related optimal flow rate.

needed to move the fluid in the heat exchanger (Eq. (16)) employing a conversion coefficient α, similarly to [43].

$$C(\dot{V},T) = P_{th}(\dot{V},T) - \alpha P_{el,c}(\dot{V}) \tag{16}$$

While the choice of the value of α can be arbitrary and dependent on the objectives of the system designer, the baseline controllers in this study employ a coefficient $\alpha = 6$, to ensure that during the charging/discharging cycle, without considering the thermal losses, the system uses always less than three times electrical energy than useful thermal energy discharged. With the defined system conditions an exergy interpretation of this coefficient with a Carnot factor of $1\text{-}T_{ref}/T_{in}$=0.16 would lead to a similar result (e.g. in charging considering T_{in} = 65 °C and the reference temperature T_{ref} = 12 °C as the undisturbed ground temperature).

An example of the evaluation of this objective function with the storage at two fixed temperatures, and supply temperature of 65 °C, in the in-series and in-parallel configurations is presented in Fig. 6.

4.2. Predictive operation optimization

The linearized BTES model, as presented in Eq. (12), can be used to optimize the operation of the system over a defined horizon, for planning and real-time control purposes. As the system is defined by discrete and continuous variables, the optimization results in a mixed integer programming (MIP) problem. The total heat absorbed or released by the BTES unit, P_{th}, is equal to the sum of all the elements of the output array y. A Boolean auxiliary variable $z \in \{0,1\}$ can be introduced to determine if the system is in cooling mode and can charge the storage ($z = 1$) or it requires heat and the storage should be discharged ($z = 0$).

4.2.1. Constraints

The system can only operate in one of the possible q modes or at one pump speed at a time, and this is ensured by constraining the sum of all the available operating modes indexes in the discrete array $u_d(q,k)$ to be equal to 1, as in Eq. (17).

$$\sum_p u_d(q,k) = 1; \tag{17}$$

Furthermore, if in-series modes are considered in the optimization, the possibility of activating the wrong flow direction in relation to the operation mode (e.g. fluid flowing from the centre to the periphery when discharging) should be prevented by introducing the constraints in Eq. (18).

$$\begin{cases} \delta_{d,s1} + \delta_{d,s2} + \cdots \delta_{d,sn} = 0 & \text{if } z(k) = 1 \\ \delta_{c,s1} + \delta_{c,s2} + \cdots \delta_{c,sn} = 0 & \text{if } z(k) = 0 \end{cases} \tag{18}$$

The supply temperature to the storage is also limited by constraints on the physical limits of the heat pump, and should be higher than the core of the storage volume if the BTES is being charged, and lower than the edge of storage volume if it is being discharged, as in Eq. (19).

$$\begin{cases} \underline{T}_{in} \le T_{in}(k) <= \overline{T}_{in} \\ T_{in}(k) \ge T_{11}(k) & \text{if } z(k) = 1 \\ T_{in}(k) \le T_{1n}(k) & \text{if } z(k) = 0 \end{cases} \tag{19}$$

Additionally, the heat transferred to and from the BTES must be lower than the available heat to be charged or the requested one to be discharged:

$$\begin{cases} P_{th}(k) \le P_{load}(k) & \text{if } z(k) = 1 \\ P_{th}(k) \ge P_{load}(k) & \text{if } z(k) = 0 \end{cases} \tag{20}$$

4.2.2. Objective function

The objective function aims at minimizing the annual CO2 emissions:

$$J = \sum_{k=1}^{N} (I_{CO_2}(k) P_{el,rem}(k) + I_{CO_2}(k) P_{el}(k) + \sum_p I_{CO_2}(k) R(p) u_d(q,k)) \tag{21}$$

where I_{CO_2} is the CO_2 intensity of the electricity from the grid at each time step k, $R(p)$ is the electrical consumption of the circulation pump in each operating mode and P_{el} and $P_{el,rem}$ are the electricity consumption of the heat pump to transfer the heat P_{th} to/from the BTES at a defined inlet temperature and the heat pump electricity consumption to meet the remainder of the demand of the system respectively. P_{el} is calculated as in Eq. (22).

$$\begin{cases} P_{el}(k) = \frac{P_{th}(k)}{COP_{ch}(k)} & \text{if } z(k) = 1 \\ P_{el}(k) = \frac{-P_{th}(k)}{COP_{dis}(k)} & \text{if } z(k) = 0 \end{cases} \tag{22}$$

The COP is a function of the supply temperature to the storage in both charging and discharging. For numerical tractability of the optimization a linearization of the COP (Eq. (23)) still preserving its dependence on the supply temperature and storage temperature is required and results in a non-linear integer programming problem to be solved. This type of problem can be solved by modern solvers like Gurobi [44], which can nowadays deal with bilinear systems and quadratic constraints.

$$\frac{1}{COP(k)} = aT_{in}(k) + b \tag{23}$$

Assuming a linearization appropriate for the case study system of the relationship in Eq. (25) between 25 and 65 °C for the charging COP ($COP_{ch}(k)$) (with a cold temperature equal to 6 °C as the cold water supply of the case study system), the coefficient a and b are equal to 4.608e−3 and -5.006e−3 respectively. Linearizing the same equation for the discharging COP ($COP_{dis}(k)$) with an inlet temperature between 12 and 25 °C and a hot supply temperature to the case study system equal to 65 °C, the coefficients a and b are equal to −4.929e−3 and 0.3204 respectively. These linearization coefficients can vary and depend on the equipment used as well as the operating range considered.

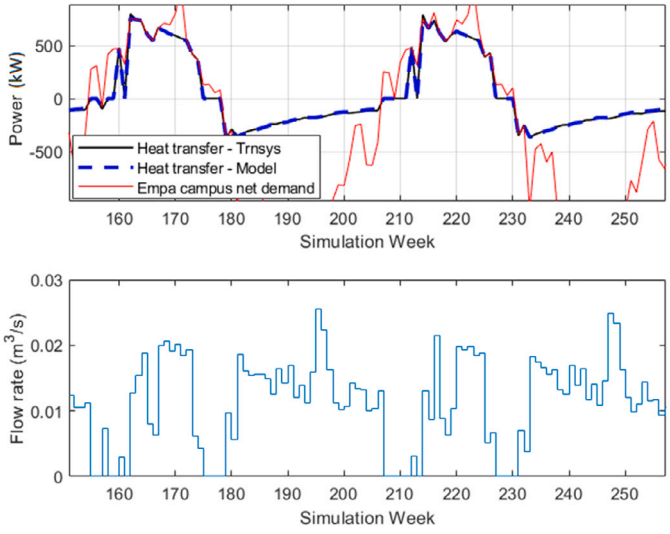

Fig. 7. Heat transfer comparison between TRNSYS and control-oriented model for an in-series configuration and optimized flow rate.

$P_{el,rem}$ is calculated as in Eq. (22), using the calculated constant COP^*_{exh} and COP^*_h, which are respectively the reference cooling exhaust COP and heating COP if the BTES is not used, determined using the relationship in Eq. (25).

$$\begin{cases} P_{el,rem}(k) = \frac{P_{load}(k) - P_{th}(k)}{COP^*_{exh}} & \text{if } z(k) = 1 \\ P_{el,rem}(k) = \frac{-P_{load}(k) + P_{th}(k)}{COP^*_h} & \text{if } z(k) = 0 \end{cases} \tag{24}$$

The temperatures used in this study for calculating the reference cooling exhaust and heating COP are presented in Section 5.

5. Implementation

5.1. Case study BTES

The BTES volume was modelled in accordance with the methodology presented in Section 3, with the objective to achieve a good prediction performance while limiting model complexity for the optimization algorithm. The model was implemented in Matlab R2019b. As in the case study BTES presented in Fig. 3 the boreholes are evenly distributed, and the in-series configuration has 18 parallel connections with 8 boreholes connected in series, the model was therefore divided in n=8 capacitances that together represent a slice of 1/18 of the total cylindrical ground volume V_{gr}. The cylinder has a depth D and a diameter D_i both equal to 51 m. The model was extended beyond D_i with volume of ground to the diameter $D_{i,end}$ equal to 66.5 m. This volume was then divided in 3 sections, linearly spacing the diameters between D_i and $D_{i,end}$, making N=11. Below the storage 2 capacitances were added (m was thus equal to 3), representing ground layers of thickness equal to 1/15 and 1/5 of D. The model used therefore had a number of states (N_{st}) equal to 33. The HTF selected was water, and the water properties were calculated at 25 °C. The simulation (and control) time step was considered to be equal to a week (168 h) to enable the possibility to optimize the operation of the storage with a horizon of one year with moderate computation time. A weekly timestep was considered an appropriate tradeoff between computational complexity and accuracy.

5.2. Model fitting and validation

The performance of the control-oriented BTES model presented in Section 3 was evaluated by a comparison of results with those obtained through simulations of the same BTES using traditional modelling methods implemented in TRNSYS. The system was simulated in TRNSYS 18.02, using a TRNSYS TYPE based on the TRNSBM [45]. This TYPE allows for almost any combination of hydraulic connections between the boreholes and offers the flexibility needed for performance optimization. The theoretical foundation of the model is the superposition method introduced in [15]. The TRNSYS model, built in accordance with the construction specification presented in Section 2 (specifically in Table 1 and in Fig. 3), was simulated with hourly time step resolution, using the same input array (fluid temperature and mass flow rate) as the one calculated by a reference controller in Matlab. An optimal instantaneous flow rate profile, used to benchmark the response of both models, was calculated using the optimization method defined Section 4.1, using an α value equal to 6 and assuming a constant supply temperature in charging of 65 °C and 12 °C in discharging. An example of the resulting cost function evaluated with the storage at 12 °C and 40 °C in the in-series and in-parallel configurations, is presented in Fig. 6.

The simulation length was set to 5 years, repeating each year the profile in Fig. 2. The resistance per meter length of ground heat exchanger pipe $R_{b,id}$ was identified to be equal to 1.477 K/m W, a value obtained by minimizing the RMSE over the two datasets, as presented in Section 3. The RMSE value between the two signals was 11.5 kW and 22.8 kW for these two datasets respectively. The difference between the modelled heat transfer and the resulting one from the TRNSYS simulations is presented in Fig. 7, showing two years of operation in an in-series configuration.

The TRNSYS simulation was set to return in its results three horizontal sections of the BTES volume, with the average temperature in a 50X50 elements matrix. These were calculated at three different depths, 10, 25 and 40 meters and averaged. Using the same 8 radial delimitations presented in Fig. 3, the average temperature in each volume was calculated. This enables a direct comparison between the 8 activated capacitances (C_{11} to C_{18}) of the model implemented in Matlab, and a comparison of the temperature profiles of the first (core), third (middle) and seventh (edge) capacitances, as shown in Fig. 8.

It can be noticed that the control-oriented model has a very similar dynamical response to the more detailed TRNSYS model, with the largest error found in the first year, likely due to the approximations the control-oriented model (e.g. not taking into account the short term dynamics of the ground near the borehole), and at the edge of the storage. The latter could be due to the fact that the rings delimiting the volumes in which the temperature is averaged might not contain the exact expected number of boreholes. The accuracy of the control-oriented model in comparison to the TRNSYS one can also be seen from the summary of the results presented in Table 2, where the average yearly charged heat, discharged heat, and consequent storage efficiencies are compared. These results were averaged over the first two and the last three years of simulation. As expected from the comparison of the temperature response of the two models, the error made by the control-oriented model in the first two years is larger than in the last three, when the ground temperature swing stabilizes, but is still relatively small, in the order of 2%–6%. After the first two years of operation, the error was less than 1% in both the charged and discharged energy, with a slightly higher underestimation of the discharged heat, leading to a modest underestimation of the efficiency of the storage. Nevertheless, the error on the efficiency estimation was also less than 1%. The results in Table 2 also show that the optimization of the flow rate is effective in maintaining a low system pumping power in comparison to the heat exchanged in the storage, maintaining the pumping energy at roughly 0.7% and 1.1% of the thermal energy extracted yearly in the in-parallel and in-series scenarios respectively, leading to a ratio between the discharged thermal energy and pumping electrical energy of around 150 for the in-parallel configuration and 90 for the in-series one.

Table 2
Yearly results comparison in the initial years (average of year 1 and 2) and during normal operation (average of year 3 to 5).

		In-series			In-parallel		
		Model	Trnsys	Error	Model	Trnsys	Error
yr.1-2	Charg. heat (MWh)	1357.4	1387.1	−2.1%	1413.9	1420.2	−0.4%
	Disch. heat (MWh)	828.5	793.7	4.4%	873.5	821.0	6.4%
yr.3-5	Charg. heat (MWh)	1380.0	1382.8	−0.2%	1466.9	1465.3	0.1%
	Disch. heat (MWh)	978.8	985.0	−0.6%	1043.0	1049.7	−0.6%
	Storage effic. (%)	0.709	0.712	−0.4%	0.711	0.716	−0.7%
	Pump energy (MWh)	10.6	10.6		7.15	7.15	
	COP	90.6	92.9		145.8	146.8	

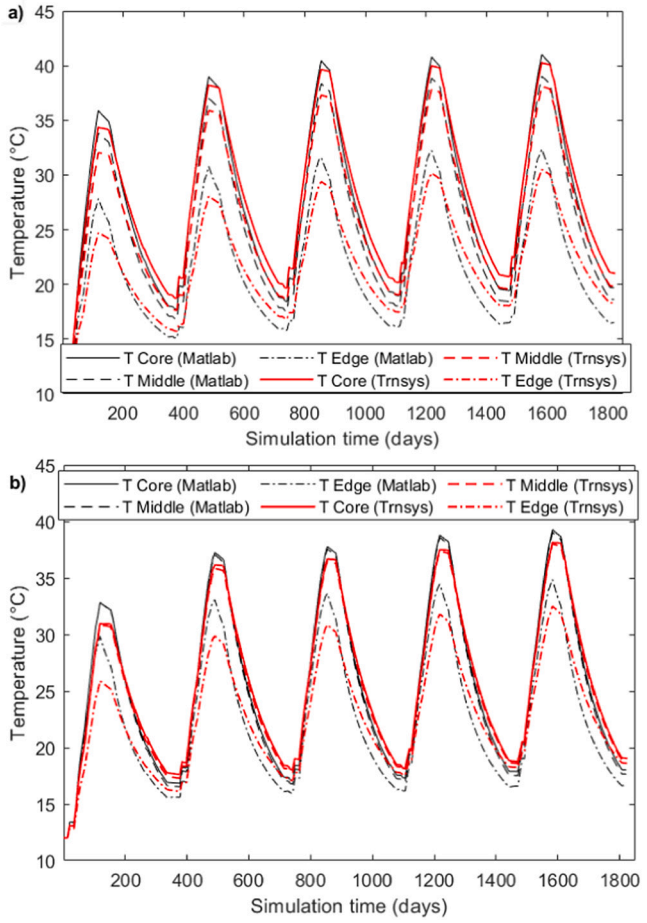

Fig. 8. BTES temperature profiles comparison between TRNSYS and control-oriented modelling, (a) in-series configuration and (b) in-parallel configuration.

Through comparison with current best-practice approaches to BTES simulation methods, the optimization-oriented model was considered accurate enough for its purpose, especially considering that it was limited to weekly computational resolution (while the model in TRNSYS was computed with hourly resolution) and to only 33 thermal nodes.

5.3. Operational optimization and controllers performance benchmarking

To evaluate the effectiveness of the optimization strategy and how the storage should be operated under different boundary conditions, the following benchmarking methodology was utilized. A five-year simulation was performed for all the scenarios studied. The total yearly CO_2 emissions, the key performance indicator, was calculated as the sum of all the electrical consumption from the various sources multiplied by the CO_2 intensity at each time-step k, in the same way as in Eq. (21), for the fifth year of operation. Electricity was used by the system in three ways, all included in this cost function: (i) the heat generated and transferred to/from the storage, (ii) the remaining heating and cooling to be provided by the heat-pump without the use of the BTES and (iii) the power required for the water to be circulated in the GHXs. For the conversion of the heat in points (i) and (ii), the following non-linear relationship in Eq. (25), based on a constant exergy efficiency, was used:

$$COP_{ch} = 0.6\frac{T_h}{T_h - T_c} \tag{25}$$

where T_h and T_c are the hot and cold reservoir temperatures in Kelvin. In charging mode, T_h is equal to the inlet temperature to the BTES T_{in}, and T_c is equal to the cold water supply temperature to the system, which for the case study was equal to the 6 °C of the cooling network. In discharging T_h is equal to the supply of hot water temperature of the system, which in this case was equal to 65 °C, and T_c is equal to T_{in}. When the BTES is not used, the exhaust temperature for the cooling operation is assumed to be equal to 35 °C, and the ambient temperature for heating operation equal to 1 °C. The operation of the BTES was tested for each plumbing configuration (in-series and in-parallel) and employing four control approaches: three baseline controllers with constant charging/discharging temperatures and variable flow rate, as presented in Section 4.1, and one optimized controller with variable charging and discharging temperatures, as presented in Section 4.2. In addition, a controller with the possibility to operate in "mixed-mode", where the plumbing configuration could be dynamically changed from parallel to in-series and vice versa, was also considered. A scenario where no BTES is integrated into the energy system, where all the heat is rejected and sourced at the aforementioned fixed temperatures, was also considered as a reference.

A summary of all the 9 control scenarios analysed in this study, together with the scenario without a BTES, is presented in Table 3.

These scenarios were evaluated using the current typical CO_2 intensity profile for Switzerland's electricity network. A second scenario was also evaluated, employing a modified CO_2 intensity profile that may represent an increase in on-site electrical solar generation in summer. This profile was created by assuming the CO2 intensity to be heavily reduced (by 2/3 of the original value) during the charging (cooling dominated) weeks. The reduced intensity CO2 profile used for this second set of simulations is shown in Fig. 9.

Using the aforementioned α setting of 6, the average ratio between the useful thermal energy discharged and electrical energy used over a year is between 90 and 150 as previously presented in Table 2. For comparison, in the in-series configuration, setting the value of $\alpha = 2$ leads to less than 1% additional energy extracted from the storage yearly, but reduces the ratio between this thermal energy and the electricity used for pumping to approximately 35.

The optimal controllers were evaluated by performing an open-loop optimization of the system operation in the fifth year, using a control time-step of one week and a prediction horizon of 52 weeks. The defined CO_2 intensity and demand profile P_{load} were used by the control to calculate the optimal control sequence. The demand profile

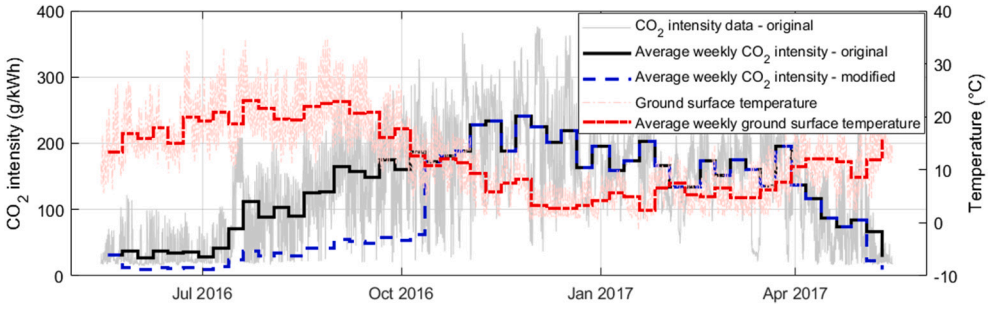

Fig. 9. Original and modified CO_2 profiles.
Source: From [7].

Table 3
Simulation scenarios summary description.

Scenario	Description	Charging temp.	Disch. temp.	Pump speed
No BTES	No BTES integrated in the energy system	–	–	–
Base Series 65/12	Baseline control, in-series config.	65 °C	12 °C	Variable
Base Series 65/20	Baseline control, in-series config.	65 °C	20 °C	Variable
Base Series 35/12	Baseline control, in-series config.	35 °C	12 °C	Variable
Base Parall. 65/12	Baseline control, in-parallel config.	65 °C	12 °C	Variable
Base Parall. 65/20	Baseline control, in-parallel config.	65 °C	20 °C	Variable
Base Parall. 35/12	Baseline control, in-parallel config.	35 °C	12 °C	Variable
Optimal Series	Optimal control, in-series config.	Variable ≤ 65 ° C	Variable ≥ 12° C	2 fixed
Optimal Parall.	Optimal control, in-parallel config.	Variable ≤ 65 ° C	Variable ≥ 12° C	2 fixed
Optimal Mixed	Optimal control, mixed-mode config.	Variable ≤ 65 ° C	Variable ≥ 12° C	1 fixed for each mode

was limited to ±900 kW, as this is the BTES heat transfer limit in the most favourable conditions and it may not able to absorb additional power. The initial condition used for this evaluation was retrieved from the simulation of the best performing baseline controller, using the last set of states at the end of the 4th year. Differently from the baseline controllers, the pump speed had to be discretized in this case, and only a limited number of speeds could be considered. The discrete flow rates considered, which were derived from the operation range resulting from the baseline controllers, are reported in Table 4, with the relative calculated pumping energy.

A machine with an 8th generation Intel i7 processor (6 cores) and 32GB of RAM was used to conduct this study. The model was developed in Matlab, using the Yalmip toolbox [46] and Gurobi v9.1 [44] was used as a solver for the optimization. A maximum time for finding the optimal solution was set to 2 h, to enable a realistic implementation, and as the MIP gap would reduce slowly after the first hour of optimization. In all the optimization scenarios the MIP gap was in the range of 3%–5% when the maximum time was reached, indicating the solution provided is effectively near-optimal.

6. Results and discussion

The results presented in this section were obtained by performing simulations using the methodology presented in Section 5, comparing the various scenarios in the fifth year of operation of the BTES storage. The BTES thermal behaviour in the various control scenarios is shown in Table 5, presenting the heat charged to the BTES along with the percentage of total available heat for charging (resulting from the cooling demand rejection), as well as the heat discharged from the BTES and the percentage of the campus total heat demand, and the resulting BTES efficiency (defined as the ratio between energy discharged and energy charged). The total available heat for charging, rejected from the cooling operation, was equal to 1877.6 MWh/y, and the total demand for heat was equal to 4887.1 MWh/y.

The summary of the performance of the studied control scenarios in terms of yearly CO_2 emissions and difference from the case without a BTES implemented is shown for both the standard and modified CO_2 intensity profile, along with the total electricity consumption, in Table 6.

The results from these simulations highlight that the CO_2 intensity profile is crucially important in determining the best BTES operation strategy. Observing in Fig. 10 the total CO_2 emission obtained using the standard CO_2 emission intensity profile it can be noticed that, between scenarios employing a baseline control, the low-temperature ones (35/12) achieve the best performance, with the in-series and in-parallel configuration obtaining similar results. It can also be noticed that a high-temperature BTES is not beneficial in this CO_2 intensity profile case, even in comparison to the case without a BTES storage: the reduction of CO_2 intensity in summer is not sufficient to compensate the higher energy consumption of the baseline operating at higher charging temperature (65/12 and 65/20), as shown in Table 6. The low-temperature baseline controllers used less electrical energy compared to the scenario without a BTES (Table 6). This is to be expected as the baseline controllers charge the BTES at the same temperature as the heat pump would reject the waste heat when cooling, allowing the system to reclaim some of this heat during winter. Similarly, the optimal controllers used less electrical energy.

Fig. 10 shows that the optimization methodology proposed in this paper outperforms the baseline controllers in terms of annual CO_2 emissions in both the in-series and in-parallel scenarios. The best optimal controller, in this case, was the one that allowed the switching between operating modes (Opt. Mixed).

The results from the simulations employing a further reduced summer CO_2 intensity profile were significantly different, favouring controllers operating the BTES at higher temperatures. This can also be observed in Fig. 10 where, between the baseline controllers, the high-temperature ones (65/20 °C) obtained the lowest yearly CO_2 emissions. This was achieved despite having the highest thermal losses (lowest storage efficiency, as reported in Table 5) as the temperature of the BTES is higher on average over the course of the year. In this CO_2 intensity profile case, differently from the case employing the standard CO_2 intensity profile, all the control scenarios employing a BTES perform

Table 4
Discrete flow rates considered in the predictive optimization.

Discrete speed	Flow-rate (m^3/s)	Consumption (kW)	Opt series	Opt paral.	Opt mixed
$\delta_{c,s1}, \delta_{d,s1}$	0.015	0.091	X		
$\delta_{c,s2}, \delta_{d,s2}$	0.010	0.03	X		X
$\delta_{p,1}$	0.120	0.101		X	
$\delta_{p,2}$	0.080	0.03		X	X

Table 5
Yearly thermal energy results comparison between baseline and optimal controllers, standard (std) and modified (mod) CO2 profiles.

	Heat charged (MWh/y)	%of Avail. heat	Heat discharged (MWh/y)	%of Avail. demand	Efficiency BTES
B. Series 65/12	1365.4	72.7%	971.4	19.9%	71.1%
B. Series 65/20	1326.9	70.7%	763.6	15.6%	57.5%
B. Series 35/15	757.4	40.3%	533.2	10.9%	70.4%
B. Par. 65/12	1482.9	79.0%	1054.4	21.6%	71.1%
B. Par. 65/20	1387.8	73.9%	817.9	16.7%	58.9%
B. Par. 35/15	812.40	43.3%	564.6	11.6%	68.8%
Opt Ser (std)	754.8	40.2%	526.5	10.8%	69.8%
Opt Par (std)	892.4	47.5%	633.0	13.0%	71.0%
Opt Mix (std)	851.7	45.4%	602.2	12.3%	70.7%
Opt Ser (mod)	1108.3	59.0%	745.3	15.3%	67.2%
Opt Par (mod)	1505.4	80.2%	1004.5	20.6%	66.7%
Opt Mix (mod)	1460.3	77.8%	983.9	20.1%	67.4%

Table 6
Yearly CO_2 and electrical energy results comparison between baseline and optimal controllers, standard (std) and modified (mod) CO2 profiles. Worst and best performing baseline controllers in each CO2 profile scenario highlighted in light red and green respectively, best performing controllers highlighted in dark green.

	CO2 (std) (t_{CO_2}/y)	CO2 (std) diff.	CO2 (mod) (t_{CO_2}/y)	CO2 (mod) diff.	El. Energy (MWh/y)	El. Energy diff.
No BTES	285.0	0%	268.5	0%	1836.1	0%
B. Series 65/12	293.5	3.0%	265.7	-1.0%	1992.6	8.6%
B. Series 65/20	288.0	1.1%	261.1	-2.7%	1957.1	6.6%
B. Series 35/15	281.1	−1.4%	264.3	−1.6%	1818.6	−1.0%
B. Par. 65/12	291.4	2.2%	264.4	-1.5%	1969.0	7.2%
B. Par. 65/20	286.0	0.3%	259.7	-3.3%	1940.2	5.7%
B. Par. 35/15	280.7	−1.5%	264.1	−1.6%	1814.4	−1.2%
Opt Ser (std)	279.6	−1.9%			1810.2	−1.4%
Opt Par (std)	279.1	−2.1%			1812.7	−1.3%
Opt Mix (std)	278.7	-2.2%			1808.1	−1.5%
Opt Ser (mod)			259.6	−3.3%	1868.9	1.8%
Opt Par (mod)			257.3	−4.2%	1910.7	4.1%
Opt Mix (mod)			257.1	-4.3%	1900.6	3.5%

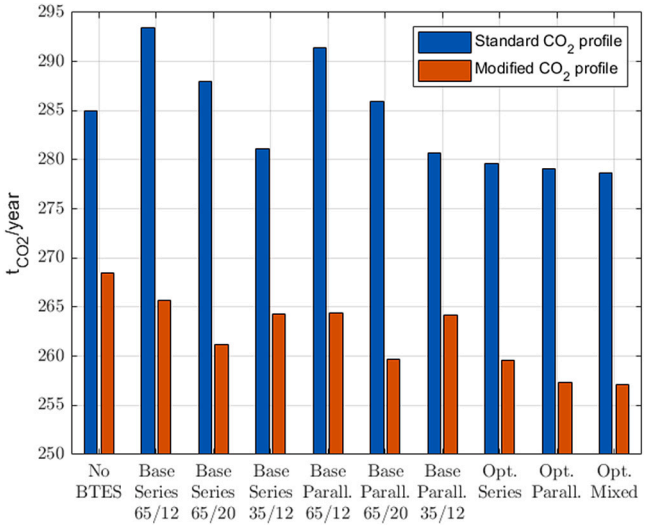

Fig. 10. Yearly CO2 emission in the various scenarios.

better than the scenario without one. Also in this case it can be seen that the optimization methodology proposed outperformed the baseline controllers in terms of yearly CO_2 emissions in both the in-series and in-parallel configurations, with the mixed-mode one achieving again the best result.

The temperature evolution of the BTES when the optimal in-series controllers were employed (in both the standard and modified CO_2 cases) is presented in Fig. 11, together with the control inputs sequence (supply temperatures and HTF flow rates).

In the standard CO_2 case, the optimal controller had a very similar behaviour to the Baseline 35/12 one in terms of BTES temperature swing. The charging temperature was slightly higher than the baseline 35 °C at the beginning of the charging operation, when also the CO_2 intensity was lower (see Fig. 9), enabling a higher supply temperature (and therefore COP) at the beginning of the discharging operation.

In the modified CO_2 case the optimal BTES swing was more similar to one of the Baseline 65/20 scenario, but with a reduced peak temperature. The charging phase was done at the higher pump speed for the majority of the time, the supply temperature was increased from 50 °C to the highest boundary of 65 °C after the first 6 weeks, but subsequently reduced as the core of the BTES became warmer. The discharging phase, undertaken mostly with the lower pump speed, the supply temperature is gradually and almost linearly decreased from

24 °C to 13 °C, to take advantage of a higher heat pump COP while the BTES is at warmer temperatures.

The evolution of the BTES temperature when the optimal in-parallel controllers were employed is shown in Fig. 12. In the standard CO_2 case the optimal controller behaved again similarly to the Baseline 35/12 scenario, but with a slightly higher temperature swing, as a result of a slightly higher inlet temperature throughout the charging phase.

In the modified CO_2 intensity profile case, the optimal controller followed again a similar trend to the Baseline 65/20 scenario, but in this case reaching a similar peak temperature. This was also achieved, in the charging phase, by increasing the supply temperature increasing to 65 °C after the first 6 weeks, but remaining relatively higher in comparison to the in-series configuration for the remainder of the charging phase. A similar linear decay of the inlet temperature was noticeable in the discharging phase results, but more pronounced, from 28 °C to 12 °C.

In the optimal mixed-mode operation scenarios, where the switch between in-series and in-parallel operation was allowed, are presented in Fig. 13. In the standard CO_2 intensity profile case, the optimal controller decided to utilize the in-parallel operation most of the time, switching to the in-series operation only in a few instances, at the end of the charging phase at the beginning of the discharging one. The supply temperature and resulting BTES temperature profile were therefore very similar to the ones of the optimal in-parallel controller.

In the modified CO_2 intensity profile case the optimal controller made more extensive use of the in-series operation, especially in the charging phase, possibly to increase the temperature gradient in the BTES and reduce the losses.

In general, considering the standard CO_2 intensity profile results (Table 6), the reduction in CO_2 emissions compared to the case without BTES was limited. In the best case scenario the reduction was equal to 2.2%, and this was due to the fact that the heating demand of the Empa campus is significantly larger than the cooling one, and the BTES is undersized compared to the demand if it is operated in a small temperature range as in a low-temperature BTES. This can be seen in see Table 5, where the best performing controller (optimal, mixed-mode operation) could only cover 12.3% of the heating demand of the Empa campus, storing 45.4% of the available rejected heat from the cooling operations. This means that the majority of the heating and cooling demand cannot be shifted by BTES, leading to a relatively small reduction of the total CO_2 emissions. From the same table it can be observed that this solution allows the BTES to perform efficiently, with an expected storage efficiency of 70.7%. It should be also noted that the reported performance increase of the best optimal controller (optimal, mixed-mode operation) in comparison to the best baseline controller (Baseline parallel 35/12) was approximately 50% higher (1.4-1.5% of the low-temperature baseline controllers compared to 1.9-2.2% of the optimized controllers).

Considering the modified CO_2 intensity profile results (Table 6), the reduction in emission was more significant. The fact that BTES was operated in a larger temperature range increased its capacity. In the best case control scenario (optimal, mixed-mode operation) the emissions were reduced by 4.3%. As reported in the same table, this result was achieved despite a higher energy consumption compared to the case without a BTES storage, as the benefit was taken from the larger difference in CO_2 intensity between summer and winter. This solution enabled the BTES to operate with a storage efficiency of 67.4%. In this best case control scenario the BTES could still supply a limited amount of the total heat demand (20.1%), but could absorb a larger fraction of the heat to be rejected from the cooling operation (77.8%), as reported in Table 5.

6.1. Emissions reduction associated with the BTES operation

A further calculation was undertaken to estimate the potential reduction in CO2 emission from a BTES appropriately sized for a more

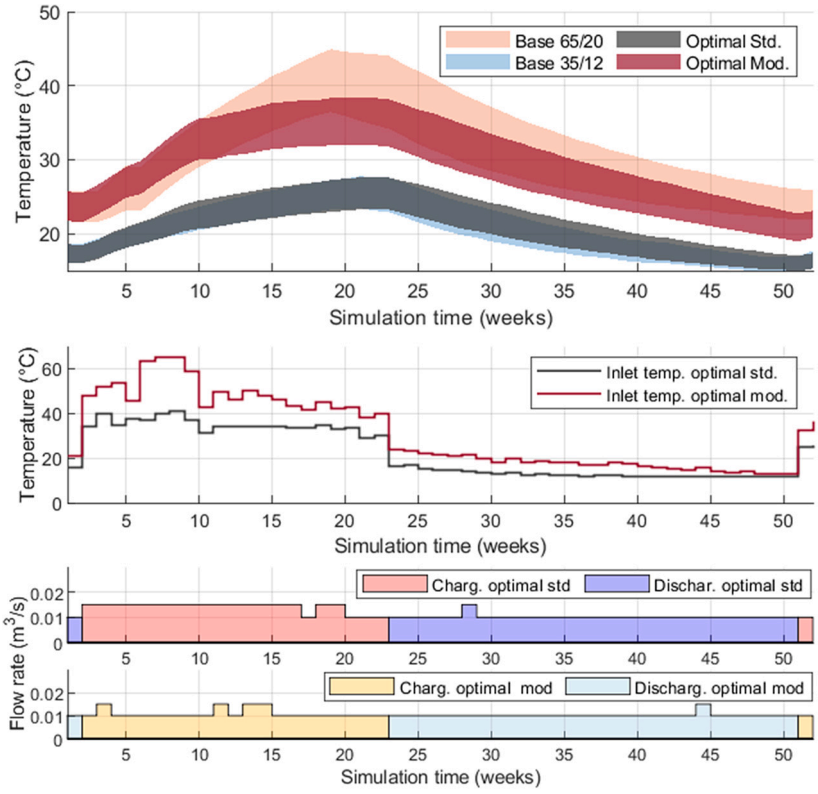

Fig. 11. BTES temperature range (above) of the baseline controllers and optimal ones (with standard and modified CO_2 profile) employing the in-series configuration; and (below) supply temperature profile and flow rate management of the optimal controllers.

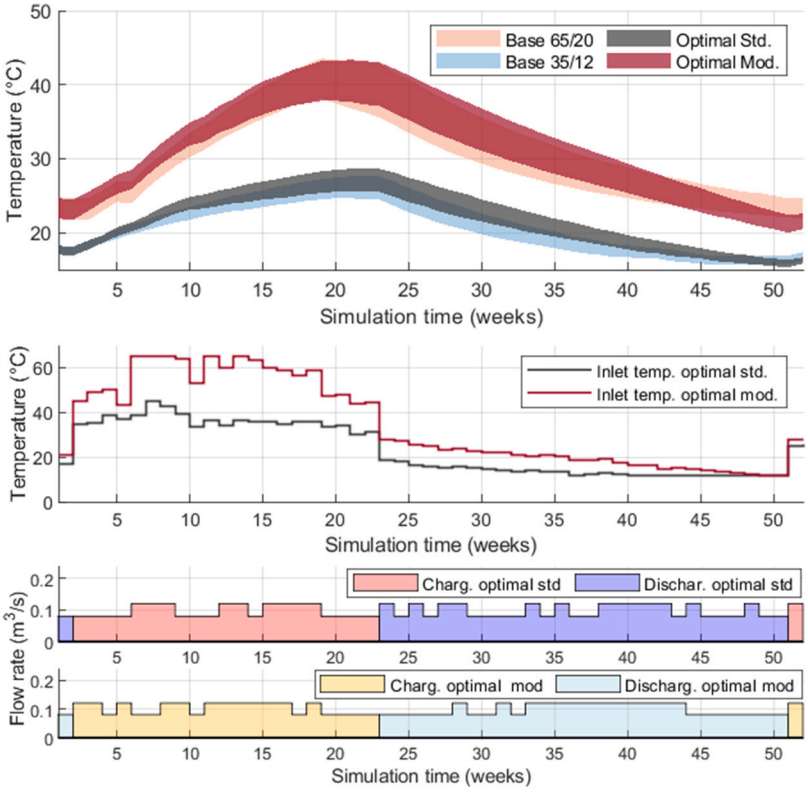

Fig. 12. BTES temperature range (above) of the baseline controllers and optimal ones (with standard and modified CO_2 profile) employing the in-parallel configuration; and (below) supply temperature profile and flow rate management of the optimal controllers.

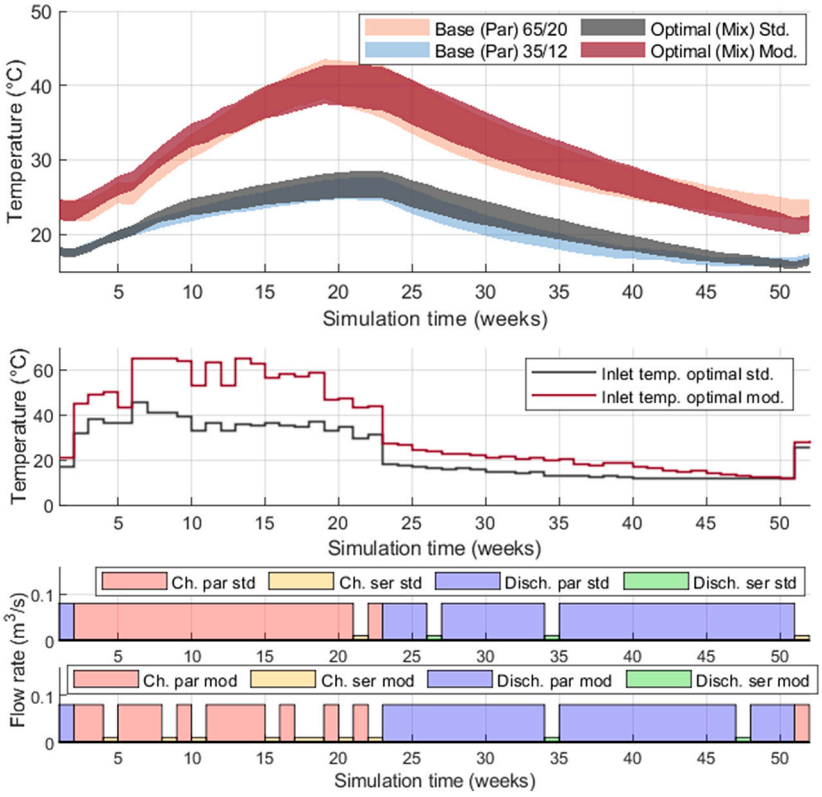

Fig. 13. BTES temperature range (above) of the baseline controllers (in-parallel configuration) and optimal ones (with standard and modified CO_2 profile) employing the mixed-mode configuration; and (below) supply temperature profile and flow rate management of the optimal controllers.

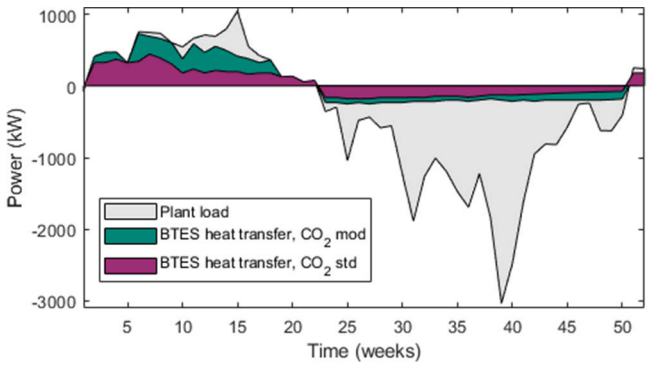

Fig. 14. BTES heat transfer, in-parallel configuration, optimized operation. Positive power corresponds to BTES charging, negative to discharging.

Table 7
Yearly CO2 emissions and reduction relative to the portion of heating and cooling covered by the BTES in each optimal control case and CO_2 intensity profile scenario.

	Base emissions (t_{CO_2}/y)	Opt. ctrl. emissions (t_{CO_2}/y)	CO_2 difference
Opt Ser (std)	38.5	33.1	13.9%
Opt Par (std)	45.9	40.1	12.8%
Opt Mix (std)	43.5	37.2	14.5%
Opt Ser (mod)	44.6	35.7	19.9%
Opt Par (mod)	60.5	49.4	18.4%
Opt Mix (mod)	59.4	47.9	19.2%

balanced heating and cooling demand, or the addition of an external heat source during summer. To this end, the CO_2 emissions of only the heating and cooling provided by the BTES in each optimal control scenario were calculated, and compared to the emissions of the same heating and cooling demand profiles provided by the base system without a BTES. An example of the charging and discharging operations considered is provided in Fig. 14, where the optimal in-parallel controller case is presented.

The calculated reduction of CO_2 emissions using the three optimal control approaches under the two considered CO_2 intensity profiles is reported in Table 7.

As it can be noticed from this table, the effective reduction of CO_2 emissions of the BTES is in the order of 13%–14% in the standard CO_2 intensity profile scenario, and in the order of 18%–20% in the modified CO_2 intensity profile scenario, hinting that with a more balanced heating and cooling demand and with better sized BTES, larger CO_2 reductions are possible. When considering these results, it should be noted that the potential presence of groundwater flow, detrimental to the efficiency of the storage, was not modelled.

7. Conclusions

This paper has provided an effective modelling and optimization methodology for the operation of a BTES. The proposed modelling method, based on a resistance–capacitance (R–C) equivalence and linearized heat transfer calculation within the boreholes, was successfully calibrated and validated against a high-fidelity Trnsys model. This model was then utilized to optimize the performance of a BTES system based on a case study where its design, historical operational data, and the electricity CO_2 emission intensity profile, were used to determine whether a benefit in terms of yearly CO_2 emissions reduction could be achieved using seasonal thermal energy storage. The optimization determined the best operating conditions (e.g. system inlet temperature and flow rate in the charging and discharging phases) with a weekly control time-step and a yearly horizon. The performance of the optimal controllers in each plumbing configuration (in-series and in-parallel) was benchmarked against a set of baseline controllers employing fixed charging and discharging inlet temperatures and variable flow rate. An additional optimal controller was also tested, allowing the system to switch during the operation between the in-series and in-parallel configurations. These control approaches were tested under two different electricity CO_2 intensity profiles, a standard one and a second one with reduced intensity during cooling dominated periods. The implementation of the proposed optimization method showed that a) the predictive optimization approach, with a more limited range of available flow rates, but with the possibility to dynamically change the supply temperature, always outperforms the baseline controllers and b) the calculated optimal solution is effective in adapting to the changing boundary conditions, as the electricity CO_2 intensity profile, modifying the supply temperature in charging and discharging to achieve the best result.

This was evident as under the standard intensity profile conditions, a lower temperature BTES would perform better, while in the modified emission intensity profile scenario, the optimal operation of the BTES would require a higher supply and discharge temperature, resulting in higher temperature swing.

The results show that the optimal controllers could take advantage of the BTES and changes in seasonal CO_2 intensity to reduce the yearly CO_2 emissions of the system by 2.2% with the standard CO_2 intensity profile and by 4.3% with the modified CO_2. The limited reduction is attributable to the fact that the cooling and heating demands of the case study are not balanced, with a heating demand being significantly larger than the cooling one, and the storage being small in comparison to the demand. Nevertheless, considering only the emissions associated with the heating and cooling provided via the BTES in the various optimal control scenario and comparing them with the emissions from the base system, a reduction in the range of 12.8%–19.9% was calculated. Furthermore, the proposed optimization strategy achieved a reduction in yearly emissions approximately 50% higher than the best performing standard controller.

As an outlook for future work, this control-oriented model has the potential to be applied to real systems as its parameters can be identified using experimental data, providing more flexibility, and potentially better prediction possibilities than a classical white-box approach. This possibility to tune the model parameters could also help overcoming the limitation of this study in considering groundwater flow. Shorter control-time steps can also be evaluated as part of the optimization framework (e.g. employing a hierarchical approach), which could enable the system to further reduce its yearly CO_2 emissions by exploiting the higher frequency variations in CO_2 emissions intensity of the electricity.

From a system perspective, it is also assumed that CO2 emission can be further reduced through optimal sizing of the BTES and incorporation of additional renewable energy sources such as solar thermal collectors, and a larger benefit might be present if newer buildings with lower heating supply temperatures are considered to be served. In future, additional consideration of the economic dimension will help to deduce further recommendations towards BTES design and implementation.

Declaration of competing interest

The authors declare that they have no known competing financial interests or personal relationships that could have appeared to influence the work reported in this paper.

Acknowledgements

We acknowledge the assistance with the TRNSYS simulations as well as valuable insights and guidance of our colleague R. Weber. This

research work was financially supported by the Swiss Federal Office of Energy SFOE, Switzerland grant Nr. SI/501938-01.

References

[1] International Energy Agency, Technology Roadmap - Solar heating and cooling, Tech. rep, 2012.

[2] A. Dahash, F. Ochs, M.B. Janetti, W. Streicher, Advances in seasonal thermal energy storage for solar district heating applications: A critical review on large-scale hot-water tank and pit thermal energy storage systems, Appl. Energy 239 (2019) 296–315, http://dx.doi.org/10.1016/j.apenergy.2019.01.189.

[3] S.K. Shah, L. Aye, B. Rismanchi, Seasonal thermal energy storage system for cold climate zones: A review of recent developments, Renew. Sustain. Energy Rev. 97 (July) (2018) 38–49, http://dx.doi.org/10.1016/j.rser.2018.08.025.

[4] D. Mangold, L. Deschaintre, Seasonal thermal energy storage - Report on state of the art and necessary further R + D, IEA-SHC Task 45 Large Systems (2015) 1–48, http://task45.iea-shc.org/data/sites/1/publications/IEA_SHC_Task45_B_Report.pdf.

[5] S. Buffa, M. Cozzini, M. D'Antoni, M. Baratieri, R. Fedrizzi, 5th generation district heating and cooling systems: A review of existing cases in Europe, Renew. Sustain. Energy Rev. 104 (2019) 504–522, http://dx.doi.org/10.1016/j.rser.2018.12.059.

[6] A. Hesaraki, S. Holmberg, F. Haghighat, Seasonal thermal energy storage with heat pumps and low temperatures in building projects—A comparative review, Renew. Sustain. Energy Rev. 43 (2015) 1199–1213, http://dx.doi.org/10.1016/j.rser.2014.12.002.

[7] electricitymap, https://www.electricitymap.org/map.

[8] R. Weber, L. Baldini, High temperature seasonal BTES for effective load shifting and CO2 emission reduction, in: Eurosun 2018 – 12th International Conference on Solar Energy for Buildings and Industry., no. September, Rapperswil, Switzerland, 2018, pp. 1–9, http://dx.doi.org/10.18086/eurosun2018.13.04.

[9] B. Nordell, G. Hellström, High temperature solar heated seasonal storage system for low temperature heating of buildings, Sol. Energy 69 (6) (2000) 511–523, http://dx.doi.org/10.1016/S0038-092X(00)00120-1.

[10] B. Sanner, K. Knoblich, Advantages and problems of high temperature underground thermal energy storage, Bulletin d'Hydrogéologie 17 (1999) 341–348.

[11] B. Sibbitt, D. McClenahan, R. Djebbar, J. Thornton, B. Wong, J. Carriere, J. Kokko, The performance of a high solar fraction seasonal storage district heating system – five years of operation, Energy Procedia 30 (2012) 856–865, http://dx.doi.org/10.1016/j.egypro.2012.11.097.

[12] L. Mesquita, D. McClenahan, J. Thornton, J. Carriere, B. Wong, Drake landing solar community: 10 years of operation, in: ISES Solar World Congress 2017 - IEA SHC International Conference on Solar Heating and Cooling for Buildings and Industry 2017, Proceedings, International Solar Energy Society, 2017, pp. 333–344, http://dx.doi.org/10.18086/swc.2017.06.09.

[13] J. Nußbicker-Lux, The BTES project in Crailsheim (Germany) - Monitoring results, 2012.

[14] T. Persson, O. Stavset, R.K. Ramstad, M.J. Alonso, K. Lorenz, Software for modelling and simulation of ground source heating and cooling systems, Tech. rep., Sintef, 2016, www.sintef.no/energi.

[15] P. Eskilson, J. Claesson, Simulation model for thermally interacting heat extraction boreholes, Numer. Heat Transfer 13 (2) (1988) 149–165, http://dx.doi.org/10.1080/10407788808913609.

[16] J. Nussbicker, W. Heidemann, H. Müller-Steinhagen, Validation of a computer model for solar coupled district heating systems with borehole thermal energy store, Effstock 2009, 2009.

[17] P. Pärisch, O. Mercker, P. Oberdorfer, E. Bertram, R. Tepe, G. Rockendorf, Short-term experiments with borehole heat exchangers and model validation in TRNSYS, Renew. Energy 74 (2015) 471–477, http://dx.doi.org/10.1016/J.RENENE.2014.07.052.

[18] G. Hellström, B. Sanner, Earth energy designer (EED). User's manual, Version 3.2, Lund University, 2015.

[19] M. Cimmino, Semi-analytical method for g-function calculation of bore fields with series- and parallel-connected boreholes, Sci. Technol. Built Environ. 25 (8) (2019) 1007–1022, http://dx.doi.org/10.1080/23744731.2019.1622937.

[20] A. Laferrière, M. Cimmino, D. Picard, L. Helsen, Development and validation of a full-time-scale semi-analytical model for the short- and long-term simulation of vertical geothermal bore fields, Geothermics 86 (2020) 101788, http://dx.doi.org/10.1016/j.geothermics.2019.101788.

[21] J. Formhals, H. Hemmatabady, B. Welsch, D.O. Schulte, I. Sass, A modelica toolbox for the simulation of borehole thermal energy storage systems, Energies 13 (9) (2020) http://dx.doi.org/10.3390/en13092327.

[22] D.O. Schulte, W. Rühaak, S. Oladyshkin, B. Welsch, I. Sass, Optimization of medium-deep borehole thermal energy storage systems, Energy Technol. 4 (1) (2016) 104–113, http://dx.doi.org/10.1002/ente.201500254.

[23] R. Franke, Object-oriented modeling of solar heating systems, Sol. Energy 60 (3–4) (1997) 171–180, http://dx.doi.org/10.1016/S0038-092X(96)00156-9.

[24] T. Schütz, R. Streblow, D. Müller, A comparison of thermal energy storage models for building energy system optimization, Energy Build. 93 (2015) 23–31, http://dx.doi.org/10.1016/j.enbuild.2015.02.031.

[25] T. Başer, J.S. McCartney, Transient evaluation of a soil-borehole thermal energy storage system, Renew. Energy 147 (2020) 2582–2598, http://dx.doi.org/10.1016/j.renene.2018.11.012.

[26] N. Catolico, S. Ge, J.S. McCartney, Numerical modeling of a soil-borehole thermal energy storage system, Vadose Zone J. 15 (1) (2016) vzj2015.05.0078, http://dx.doi.org/10.2136/vzj2015.05.0078.

[27] H.S. Lim, J.S. Ok, J.S. Park, S.J. Lee, S.W. Karng, Y.T. Kang, Efficiency improvement of energy storage and release by the inlet position control for seasonal thermal energy storage, Int. J. Heat Mass Transfer 151 (2020) 119435, http://dx.doi.org/10.1016/j.ijheatmasstransfer.2020.119435.

[28] S.K. Shah, L. Aye, B. Rismanchi, Multi-objective optimisation of a seasonal solar thermal energy storage system for space heating in cold climate, Appl. Energy 268 (2020) 115047, http://dx.doi.org/10.1016/j.apenergy.2020.115047.

[29] S. Klein, TRNSYS, a Transient System Simulation Program, Solar Energy Laboratory, University of Wisconsin–Madison, 1979.

[30] V. Tulus, D. Boer, L.F. Cabeza, L. Jiménez, G. Guillén-Gosálbez, Enhanced thermal energy supply via central solar heating plants with seasonal storage: A multi-objective optimization approach, Appl. Energy 181 (2016) 549–561, http://dx.doi.org/10.1016/j.apenergy.2016.08.037.

[31] C.N. Antoniadis, G. Martinopoulos, Optimization of a building integrated solar thermal system with seasonal storage using TRNSYS, Renew. Energy 137 (2019) 56–66, http://dx.doi.org/10.1016/j.renene.2018.03.074.

[32] N. Rapantova, P. Pospisil, J. Koziorek, P. Vojcinak, D. Grycz, Z. Rozehnal, Optimisation of experimental operation of borehole thermal energy storage, Appl. Energy 181 (2016) 464–476, http://dx.doi.org/10.1016/j.apenergy.2016.08.091.

[33] C. Hachem-Vermette, K. Singh, Developing an optimization methodology for urban energy resources mix, Appl. Energy 269 (2020) 115066, http://dx.doi.org/10.1016/j.apenergy.2020.115066.

[34] M. Wirtz, L. Kivilip, P. Remmen, D. Müller, 5th generation district heating: A novel design approach based on mathematical optimization, Appl. Energy 260 (2020) 114158, http://dx.doi.org/10.1016/j.apenergy.2019.114158.

[35] B. Dehghan B., E. Kukrer, A new 1D analytical model for investigating the long term heat transfer rate of a borehole ground heat exchanger by green's function method, Renew. Energy 108 (2017) 615–621, http://dx.doi.org/10.1016/j.renene.2016.11.002.

[36] C. Verhelst, L. Helsen, G. Vandersteen, J. Schoukens, A linear dynamic borehole model for use in model based predictive control, Int. Conf. Energy Storage 32 (2009) 1–8, http://talon.stockton.edu/eyos/energy_studies/content/docs/effstock09/Session_10_2_UTES_Modelling/89.pdf.

[37] M. Hohmann, J. Warrington, J. Lygeros, A moment and sum-of-squares extension of dual dynamic programming with application to nonlinear energy storage problems, European J. Oper. Res. 283 (1) (2020) 16–32, http://dx.doi.org/10.1016/j.ejor.2019.10.041.

[38] P. Bayer, M. de Paly, M. Beck, Strategic optimization of borehole heat exchanger field for seasonal geothermal heating and cooling, Appl. Energy 136 (2014) 445–453, http://dx.doi.org/10.1016/j.apenergy.2014.09.029.

[39] I. Cupeiro Figueroa, D. Picard, L. Helsen, Short-term modeling of hybrid geothermal systems for model predictive control, Energy Build. 215 (2020) http://dx.doi.org/10.1016/j.enbuild.2020.109884.

[40] P. Gabrielli, A. Acquilino, S. Siri, S. Bracco, G. Sansavini, M. Mazzotti, Optimization of low-carbon multi-energy systems with seasonal geothermal energy storage: The anergy grid of ETH zurich, Energy Convers. Manage. X 8 (July) (2020) 100052, http://dx.doi.org/10.1016/j.ecmx.2020.100052.

[41] J. Hirvonen, H. ur Rehman, K. Deb, K. Sirén, Neural network metamodelling in multi-objective optimization of a high latitude solar community, Sol. Energy 155 (2017) 323–335, http://dx.doi.org/10.1016/j.solener.2017.06.040.

[42] D. Bauer, W. Heidemann, H. Müller-Steinhagen, H.-J.G. Diersch, Thermal resistance and capacity models for borehole heat exchangers, Int. J. Energy Res. 35 (4) (2011) 312–320, http://dx.doi.org/10.1002/er.1689.

[43] M. Fiorentini, P. Cooper, Z. Ma, Development and optimization of an innovative HVAC system with integrated PVT and PCM thermal storage for a net-zero energy retrofitted house, Energy Build. 94 (2015) 21–32, http://dx.doi.org/10.1016/J.ENBUILD.2015.02.018.

[44] Gurobi, Gurobi Solver, https://www.gurobi.com/products/gurobi-optimizer/.

[45] D. Pahud, A. Fromentin, J.C. Hadorn, The superposition borehole model for TRNSYS (TRNSBM), User Manuel, Internal Report, LASEN-EPFL, Lausanne, 1996.

[46] J. Löfberg, YALMIP : A Toolbox for Modeling and Optimization in MATLAB, in: Proceedings of the CACSD Conference, Taipei, Taiwan, 2004.